

Analytic gradients for equation-of-motion coupled cluster with single, double, and perturbative triple excitations

Tingting Zhao and Devin. A. Matthews*

Department of Chemistry, Southern Methodist University, Dallas, TX

E-mail: dmatthews@smu.edu

Abstract

Understanding the process of molecular photoexcitation is crucial in various fields, including drug development, materials science, photovoltaics, and more. The electronic vertical excitation energy is a critical property, for example in determining the singlet-triplet gap of chromophores. However, a full understanding of excited-state processes requires additional explorations of the excited-state potential energy surface and electronic properties, which is greatly aided by the availability of analytic energy gradients. Owing to its robust high accuracy over a wide range of chemical problems, equation-of-motion coupled-cluster with single and double excitations (EOM-CCSD) is a powerful method for predicting excited state properties, and the implementation of analytic gradients of many EOM-CCSD (excitation energies, ionization potentials, electron attachment energies, etc.) along with numerous successful applications highlights the flexibility of the method. In specific cases where a higher level of accuracy is needed or in more complex electronic structures, the inclusion of triple excitations becomes essential, for example, in the EOM-CCSD* approach of Saeh and Stanton. In this work, we derive and implement for the first time the analytic gradients of

EOMEE-CCSD*, which also provides a template for analytic gradients of related excited state methods with perturbative triple excitations. The capabilities of analytic EOMEE-CCSD* gradients are illustrated by several representative examples.

1 Introduction

The excited states of molecules exhibit a range of unique properties that are of great interest to many fields of science and technology: bioluminescence,¹ mutagenesis and carcinogenesis,² and photovoltaics and light-emitting diodes,^{3,4} and many more. These diverse electronic characteristics arise from their complex potential energy landscapes, which can be probed through optical or ultraviolet (UV) absorption. The relaxation and decay processes to the ground state, occurring via either radiative or non-radiative pathways, further contribute to their functionality and provide valuable spectroscopic insights, such as fluorescence and phosphorescence. Theoretical quantum chemistry calculations play a crucial role in facilitating the interpretation of this experimental spectroscopy data, offering a comprehensive understanding of the excited states.

Despite the inherent complexity of excited states (for example, open-shell and multi-reference character), numerous models have been developed to calculate excited state energies and properties. Generally, these models fall into two categories. The first category comprises explicitly multi-reference methods that deal with solutions spanning a space of determinants or other suitable basis functions, which aim to provide either state-selective, state-averaged, or state-universal descriptions of electronic states. A comprehensive review of these methods is available elsewhere.⁵ While these methods, such as complete active space self-consistent field (CASSCF) method,⁶ its second perturbation-corrected variant (CASPT2),⁷ and the second-order n -electron valence state perturbation theory (NEVPT2)⁸⁻¹⁰ have been highly successful, they demand a high level of expertise and familiarity with the system under investigation in order to tune the active orbital space and other calculation parameters. Additionally, interpreting the results can be a formidable challenge, as it often involves analyz-

ing many interacting configurations and orbitals.^{5,11} On the other hand, equation-of-motion coupled-cluster (EOM-CC) methods adopt a distinct approach, encompassing the entire set of multi-configurational target states within a single-reference framework. This black box theory has gained considerable popularity, owing to its favorable computational accessibility and its robust high accuracy over a wide range of chemical problems.¹² For excited states, equation-of-motion coupled-cluster with single and double excitations (EOMEE-CCSD)¹³ has become the gold standard method for the prediction of singly excited state energies and properties. The development of variants for ionization potentials (EOMIP-CCSD), electron attachment energies (EOMEA-CCSD), and spin-flip excitations (EOMSF-CCSD) has greatly extended its capability to describe doublet radicals, diradicals, triradicals, and bond breaking.^{14,15}

Energy differences and transition probabilities are the key quantities that are desirable to explain and predict the spectroscopic.¹⁶ Importantly, these quantities have to be computed at significant points in the potential energy surface(PES). The development of analytic-derivative techniques has significantly facilitated the exploration of potential energy surfaces (PESs) of molecules in their electronic ground state, essentially for all available quantum-chemical schemes.¹⁷⁻²⁷ Gradients are accessible for various multireference methods, including MCSCF,²⁸ MR-CI,^{29,30} and fully internally contracted CASPT2.³¹ Nevertheless, the efficiency of the EOM-CCSD gradient notably distinguishes itself. Analytic gradients for all the variants of EOM-CCSD methods have been documented.^{13,32-37}

While EOM-CCSD offers great accuracy for predominantly one-electron excitations, it is poor for double electron excitations.³⁸⁻⁴⁰ Efforts have been made in either iterative or non-iterative schemes to include triple excitation to improve accuracy, particularly for double-excited states,⁴¹ EOM-CCSD*,⁴² EOM-CCSD(\tilde{T}),⁴⁰ EOM-CCSDT-3,⁴⁰ EOM-CC3 (equivalent to LR-CC3 for energies),^{43,44} and EOM-CCSDT.⁴⁵ However, no analytic gradients have been published for these methods, although gradients for full EOMEE-CCSDT are available in the CFOUR program package⁴⁶ and transition dipole moments for EOM-CCSDT were re-

ported by Hirata.⁴⁷ Counter-intuitively, the analytic gradients for the non-iterative triples methods are more complicated than for iterative models, as discussed below. In this paper, we present, for the first time, detailed formulas and implementation details of analytic closed-shell EOMEE-CCSD* energy gradients. Several demonstrative applications are also discussed.

2 Theory

For convenience, in the following context $|H\rangle$ represents the set of all possible n -electron Slater determinants within a given spin-orbital basis. $|H\rangle$ can be further split into $|H\rangle = |P\rangle + |Q\rangle = |0\rangle + |G\rangle + |Q\rangle = |0\rangle + |S\rangle + |D\rangle + |Q\rangle$, where $|0\rangle$ is the reference determinant (Fermi vacuum), $|S\rangle = |^a_i\rangle$ are the singly-excited determinants, and $|D\rangle = |^{ab}_{ij}\rangle$ are the doubly-excited determinants. $|Q\rangle = |^{abc}_{ijk}\rangle + |^{abcd}_{ijkl}\rangle + \dots$, represents any determinant of excitation rank higher than two, out of which we specifically identify the triply-excited determinants $|T\rangle = |^{abc}_{ijk}\rangle$.

Briefly, the ground CCSD and excited state EOMEE-CCSD energies are given by,

$$E_{\text{CCSD}} = \langle 0 | e^{-\hat{T}} \hat{H} e^{\hat{T}} | 0 \rangle = \langle 0 | (\hat{H} e^{\hat{T}})_c | 0 \rangle = \langle 0 | \bar{H} | 0 \rangle \quad (1)$$

$$0 = \langle G | \bar{H} | 0 \rangle \quad (2)$$

$$\hat{H} = \sum_{pq} f_q^p \{a_p^\dagger a_q\} + \frac{1}{4} \sum_{pqrs} v_{rs}^{pq} \{a_p^\dagger a_q^\dagger a_s a_r\} = \hat{F} + \hat{V} \quad (3)$$

$$\hat{T} = \sum_{ai} t_i^a a_a^\dagger a_i + \frac{1}{4} \sum_{abij} t_{ij}^{ab} a_a^\dagger a_b^\dagger a_j a_i = \hat{T}_1 + \hat{T}_2 \quad (4)$$

$$E_{\text{EOM-CCSD}} = \langle 0 | \hat{L} \bar{H} \hat{R} | 0 \rangle \quad (5)$$

$$0 = \langle G | (\bar{H} - E_{\text{EOM-CCSD}}) \hat{R} | 0 \rangle \quad (6)$$

$$0 = \langle 0 | \hat{L} (\bar{H} - E_{\text{EOM-CCSD}}) | G \rangle \quad (7)$$

$$\hat{R} = r_0 + \sum_{ai} r_i^a a_a^\dagger a_i + \frac{1}{4} \sum_{abij} r_{ij}^{ab} a_a^\dagger a_b^\dagger a_j a_i = \hat{R}_0 + \hat{R}_1 + \hat{R}_2 \quad (8)$$

$$\hat{L} = \sum_{ai} l_a^i a_i^\dagger a_a + \frac{1}{4} \sum_{abij} l_{ab}^{ij} a_i^\dagger a_j^\dagger a_b a_a = \hat{L}_1 + \hat{L}_2 \quad (9)$$

where $\{\dots\}$ indicates normal ordering and $(\dots)_c$ indicates a connected operator product. The energy $E_{\text{EOM-CCSD}}$ and amplitudes \hat{R} and \hat{L} correspond to the same excited state which is otherwise unspecified, except that it should be non-degenerate. When properties of a specific excited state μ are required, we will employ the notation $E_{\text{EOM-CCSD}}(\mu)$, $\hat{R}(\mu)$, $\hat{L}(\mu)$, etc.

The perturbative third-order correction⁴⁸ to the EOMEE-CCSD energy can be written as follows, with $\omega = E_{\text{EOM-CCSD}} - E_{\text{CCSD}}$ being the EOMEE-CCSD vertical excitation energy,

$$\Delta E = \langle 0 | \hat{L} \hat{V} | T \rangle \langle T | (\omega - \hat{F})^{-1} | T \rangle \langle T | \hat{V} \hat{R}_2 + (\hat{V} \hat{T}_2 \hat{R}_1)_c | 0 \rangle \quad (10)$$

The total EOM-CCSD* energy can be written as,

$$E_{\text{EOM-CCSD}^*} = E_{\text{EOM-CCSD}} + \Delta E = \langle 0 | \hat{L} \bar{H} \hat{R} | 0 \rangle + \langle 0 | \hat{L}_3 (\omega - \hat{F}) \hat{R}_3 | 0 \rangle \quad (11)$$

$$\langle 0 | \hat{L}_3 | T \rangle = \langle 0 | \hat{L} \hat{V} (\omega - \hat{F})^{-1} | T \rangle \quad (12)$$

$$\langle T | \hat{R}_3 | 0 \rangle = \langle T | (\omega - \hat{F})^{-1} (\hat{V} \hat{R}_2 + (\hat{V} \hat{T}_2 \hat{R}_1)_c) | 0 \rangle \quad (13)$$

assuming a canonical reference determinant. Straightforward differentiation with respect to an arbitrary perturbation χ gives,

$$\begin{aligned} E_{\text{EOM-CCSD}^*}^\chi &= E_{\text{EOM-CCSD}}^\chi + \langle 0 | \hat{L}^\chi \hat{V} \hat{R}_3 | 0 \rangle + \langle 0 | \hat{L} \hat{V}^\chi \hat{R}_3 | 0 \rangle \\ &\quad - \langle 0 | \hat{L}_3 (\omega - \hat{F})^\chi \hat{R}_3 | 0 \rangle + \langle 0 | \hat{L}_3 (\hat{V} \hat{R}_2^\chi + \hat{V} \hat{T}_2 \hat{R}_1^\chi) | 0 \rangle \\ &\quad + \langle 0 | \hat{L}_3 \hat{V} \hat{R}_1 \hat{T}_2^\chi | 0 \rangle + \langle 0 | \hat{L}_3 \hat{V}^\chi (\hat{R}_2 + \hat{T}_2 \hat{R}_1) | 0 \rangle \end{aligned} \quad (14)$$

Note there is a negative sign in the term $\langle 0 | \hat{L}_3 (\omega - \hat{F})^\chi \hat{R}_3 | 0 \rangle$ as,

$$((\omega - \hat{F})^{-1})^\chi = -(\omega - \hat{F})^{-1} (\omega - \hat{F})^\chi (\omega - \hat{F})^{-1} \quad (15)$$

This term can be further expanded as follows, where for convenience we set $\delta = \langle 0 | \hat{L}_3 \hat{R}_3 | 0 \rangle$,

$$\begin{aligned} - \langle 0 | \hat{L}_3 (\omega - \hat{F})^x \hat{R}_3 | 0 \rangle &= \langle 0 | \hat{L}_3 (\hat{F}^x + E_{\text{CCSD}}^x - E_{\text{EOM-CCSD}}^x) \hat{R}_3 | 0 \rangle \\ &= \langle 0 | \hat{L}_3 \hat{F}^x \hat{R}_3 | 0 \rangle + \delta (E_{\text{CCSD}}^x - E_{\text{EOM-CCSD}}^x) \end{aligned} \quad (16)$$

E_{CCSD}^x and $E_{\text{EOM-CCSD}}^x$ can be obtained by directly differentiating the energy equations (1) and (5), respectively. Noting the amplitude equations (2), (6), and (7) and that $(\langle 0 | \hat{L} \hat{R} | 0 \rangle)^x = 0$,

$$E_{\text{CCSD}}^x = \langle 0 | \bar{H} \hat{T}^x | 0 \rangle + \langle 0 | \bar{H}^{(x)} | 0 \rangle \quad (17)$$

$$E_{\text{EOM-CCSD}}^x = \langle 0 | \hat{L} \bar{H}^{(x)} \hat{R} | 0 \rangle + \langle 0 | \hat{L} \bar{H} | Q \rangle \langle Q | \hat{R} \hat{T}^x | 0 \rangle \quad (18)$$

where $\bar{H}^{(x)} = (\hat{H}^x e^{\hat{T}})_c$.

Combining (14), (16), (17), and (18) and grouping all terms into four parts we obtain,

$$E_{\text{EOM-CCSD}}^x = \mathbf{I} + \mathbf{II} + \mathbf{III} + \mathbf{IV}$$

$$\mathbf{I} = \langle 0 | \hat{L}^x \hat{V} \hat{R}_3 | 0 \rangle \quad (19)$$

$$\mathbf{II} = \langle 0 | \hat{L}_3 (\hat{V} \hat{R}_2^x + \hat{V} \hat{T}_2 \hat{R}_1^x) | 0 \rangle \quad (20)$$

$$\mathbf{III} = \langle 0 | \hat{L}_3 (\hat{V} \hat{T}_2^x \hat{R}_1) | 0 \rangle + \langle 0 | (1 - \delta) \hat{L} \bar{H} | Q \rangle \langle Q | \hat{R} \hat{T}^x | 0 \rangle + \delta \langle 0 | \bar{H} \hat{T}^x | 0 \rangle \quad (21)$$

$$\begin{aligned} \mathbf{IV} &= \langle 0 | (1 - \delta) \hat{L} \bar{H}^{(x)} \hat{R} | 0 \rangle + \langle 0 | \hat{L}_3 (\hat{V}^x \hat{R}_2 + \hat{V}^x \hat{T}_2 \hat{R}_1) | 0 \rangle \\ &\quad + \langle 0 | \hat{L} \hat{V}^x \hat{R}_3 | 0 \rangle + \langle 0 | \hat{L}_3 \hat{F}^x \hat{R}_3 | 0 \rangle + \delta \langle 0 | \bar{H}^{(x)} | 0 \rangle \end{aligned} \quad (22)$$

The terms are grouped such that **I** depends (directly) only on \hat{L}^x , **II** depends only on \hat{R}^x , **III** depends only on \hat{T}^x , and **IV** depends only on the derivatives of integrals.

\hat{L}^x and \hat{R}^x of course depend in turn on \hat{T}^x due to the presence of \bar{H} in their definite amplitude equations. Thus, we should tackle **I** and **II** before moving on to **III**. To analyze

I, we first define a convenient intermediate, noting that \hat{L}^χ spans only the $\langle G|$ space,

$$\mathbf{I} = \langle 0| \hat{L}^\chi \hat{V} \hat{R}_3 |0\rangle = \langle 0| \hat{L}^\chi \hat{\Sigma} |0\rangle \quad (23)$$

$$\langle G| \hat{\Sigma} |0\rangle = \langle G| \hat{V} \hat{R}_3 |0\rangle \quad (24)$$

We then introduce a definition of \hat{L}^χ by differentiating (7),

$$\begin{aligned} \langle 0| \hat{L}^\chi (\bar{H} - E_{\text{EOM-CCSD}}) |G\rangle &= \langle 0| \hat{L} \hat{T}^\chi (\bar{H} - E_{\text{EOM-CCSD}}) |G\rangle - \langle 0| \hat{L} \bar{H}^{(\chi)} |G\rangle \\ &+ E_{\text{EOM-CCSD}}^\chi \langle 0| \hat{L} |G\rangle - \langle 0| \hat{L} \bar{H} |Q\rangle \langle Q| \hat{T}^\chi |G\rangle \end{aligned} \quad (25)$$

Notionally, one would utilize this definition by applying the inverse of $\langle G| \bar{H} - E_{\text{EOM-CCSD}} |G\rangle$ to both sides of the equation, yielding $\langle 0| \hat{L}^\chi |G\rangle = \langle 0| \hat{X} |G\rangle \langle G| \bar{H} - E_{\text{EOM-CCSD}} |G\rangle^{-1}$ with \hat{X} collecting all terms from the R.H.S., which then could be substituted in **I** giving $\langle 0| \hat{X} |G\rangle \langle G| \bar{H} - E_{\text{EOM-CCSD}} |G\rangle^{-1} \langle G| \hat{\Sigma} |0\rangle$. Finally, one would then define a new set of amplitudes $\langle G| \hat{Y} |0\rangle$ defined by the system of equations $\langle G| (\bar{H} - E_{\text{EOM-CCSD}}) \hat{Y} |0\rangle = \langle G| \hat{\Sigma} |0\rangle$. However, this plan is hindered by the fact that $E_{\text{EOM-CCSD}}$ is an exact eigenvalue of $\langle G| \bar{H} |G\rangle$, and thus the shifted matrix is exactly singular. This problem can be avoided by imposing an additional condition on \hat{L}^χ (and \hat{R}^χ): while the normalization condition $\langle 0| \hat{L} \hat{R} |0\rangle = 1$ ensures that $\langle 0| \hat{L}^\chi \hat{R} |0\rangle + \langle 0| \hat{L} \hat{R}^\chi |0\rangle = 0$, we can additionally require a biorthogonal form of intermediate normalization such that $\langle 0| \hat{L}^\chi \hat{R} |0\rangle = \langle 0| \hat{L} \hat{R}^\chi |0\rangle = 0$. Thus, the part of $\hat{\Sigma}$ parallel to \hat{R} is not required and can be projected out. Similarly, the fact that \hat{L} lies in the null space of $\langle G| (\bar{H} - E_{\text{EOM-CCSD}}) |G\rangle$ implies that each term on the R.H.S. of (25) is perpendicular to \hat{L} . Thus, it is sufficient and safe to employ the pseudo-inverse,

$$\begin{aligned} \langle 0| \hat{L}^\chi |G\rangle &= \langle 0| \hat{L} \hat{T}^\chi |G\rangle (\hat{I} - \langle G| \hat{R} |0\rangle \langle 0| \hat{L} |G\rangle) \\ &- \left[\langle 0| \hat{L} \bar{H}^{(\chi)} |G\rangle - E_{\text{EOM-CCSD}}^\chi \langle 0| \hat{L} |G\rangle \right. \\ &\left. + \langle 0| \hat{L} \bar{H} |Q\rangle \langle Q| \hat{T}^\chi |G\rangle \right] \langle G| \bar{H} - E_{\text{EOM-CCSD}} |G\rangle^+ \end{aligned} \quad (26)$$

$$\langle G | \bar{H} - E_{\text{EOM-CCSD}}(\mu) | G \rangle^+ = \sum_{\nu \neq \mu} \frac{\langle G | \hat{R}(\nu) | 0 \rangle \langle 0 | \hat{L}(\nu) | G \rangle}{E_{\text{EOM-CCSD}}(\nu) - E_{\text{EOM-CCSD}}(\mu)} \quad (27)$$

where the pseudo-inverse satisfies,

$$\begin{aligned} \langle G | \bar{H} - E_{\text{EOM-CCSD}} | G \rangle \langle G | \bar{H} - E_{\text{EOM-CCSD}} | G \rangle^+ &= \\ \langle G | \bar{H} - E_{\text{EOM-CCSD}} | G \rangle^+ \langle G | \bar{H} - E_{\text{EOM-CCSD}} | G \rangle &= \hat{I} - \langle G | \hat{R} | 0 \rangle \langle 0 | \hat{L} | G \rangle \end{aligned} \quad (28)$$

with \hat{I} being the identity operator.

The introduction of the pseudo-inverse now allows \hat{L}^x to be substituted into \mathbf{I} ,

$$\begin{aligned} \mathbf{I} &= \langle 0 | \hat{L} \hat{T}^x \hat{\Sigma}^\perp | 0 \rangle - \left[\langle 0 | \hat{L} \bar{H}^{(x)} | G \rangle - E_{\text{EOM-CCSD}}^x \langle 0 | \hat{L} | G \rangle \right. \\ &\quad \left. + \langle 0 | \hat{L} \bar{H} | Q \rangle \langle Q | \hat{T}^x | G \rangle \right] \langle G | \bar{H} - E_{\text{EOM-CCSD}} | G \rangle^+ \langle G | \hat{\Sigma} | 0 \rangle \\ &= \langle 0 | \hat{L} \hat{\Sigma}^\perp \hat{T}^x | 0 \rangle + \langle 0 | \hat{L} \bar{H}^{(x)} \hat{Y} | 0 \rangle - E_{\text{EOM-CCSD}}^x \langle 0 | \hat{L} \hat{Y} | 0 \rangle \\ &\quad + \langle 0 | \hat{L} \bar{H} | Q \rangle \langle Q | \hat{Y} \hat{T}^x | 0 \rangle \end{aligned} \quad (29)$$

$$\langle G | \hat{\Sigma}^\perp | 0 \rangle = \langle G | \hat{\Sigma} | 0 \rangle - \langle G | \hat{R} | 0 \rangle \langle 0 | \hat{L} \hat{\Sigma} | 0 \rangle \quad (30)$$

where we introduce an excitation operator \hat{Y} spanning $|G\rangle$ as,

$$\langle G | (\bar{H} - E_{\text{EOM-CCSD}}) \hat{Y} | 0 \rangle = - \langle G | \hat{\Sigma}^\perp | 0 \rangle \quad (31)$$

The portion of \hat{Y} parallel to \hat{R} is undefined, but it is convenient and numerically stable to require \hat{Y} be perpendicular to \hat{R} . In particular, this means that $\langle 0 | \hat{L} \hat{Y} | 0 \rangle = 0$. Finally we note that biorthogonal intermediate normalization is only one choice of uniquely determining $\langle 0 | \hat{L}^x \hat{R} | 0 \rangle$ and $\langle 0 | \hat{L} \hat{R}^x | 0 \rangle$. For example, one could require that $\langle 0 | \hat{R}^\dagger \hat{R} | 0 \rangle = 1$ which would still allow the definition of a consistent set of \hat{Y} amplitudes with a modified set of equations (involving an operator more complicated than the pseudo-inverse). Thus to avoid a loss of generality we do not assume that $\langle 0 | \hat{L} \hat{Y} | 0 \rangle = 0$ or other similar consequences of biorthogonal

intermediate normalization.

For **II**, we employ a similar strategy,

$$\mathbf{II} = \langle 0 | \hat{L}_3 (\hat{V} \hat{R}_2^\chi + \hat{V} \hat{T}_2 \hat{R}_1^\chi) | 0 \rangle = \langle 0 | \hat{\Omega} \hat{R}^\chi | 0 \rangle \quad (32)$$

$$\langle 0 | \hat{\Omega} | S \rangle = \langle 0 | \hat{L}_3 \hat{V} \hat{T}_2 | S \rangle \quad (33)$$

$$\langle 0 | \hat{\Omega} | D \rangle = \langle 0 | \hat{L}_3 \hat{V} | D \rangle \quad (34)$$

$$\begin{aligned} \langle G | \hat{R}^\chi | 0 \rangle &= - (\hat{I} - \langle G | \hat{R} | 0 \rangle \langle 0 | \hat{L} | G \rangle) \langle G | \hat{R} \hat{T}^\chi | 0 \rangle \\ &\quad - \langle G | \bar{H} - E_{\text{EOM-CCSD}} | G \rangle^+ \left[\langle G | \bar{H}^{(x)} \hat{R} | 0 \rangle \right. \\ &\quad \left. - E_{\text{EOM-CCSD}}^\chi \langle G | \hat{R} | 0 \rangle + \langle G | \bar{H} | Q \rangle \langle Q | \hat{R} \hat{T}^\chi | 0 \rangle \right] \end{aligned} \quad (35)$$

Substitution followed by the definition of another set of de-excitation amplitudes $\hat{\Pi}$ gives,

$$\begin{aligned} \mathbf{II} &= - \langle 0 | \hat{\Omega}^\perp \hat{R} \hat{T}^\chi | 0 \rangle - \langle 0 | \hat{\Omega} | G \rangle \langle G | \bar{H} - E_{\text{EOM-CCSD}} | G \rangle^+ \\ &\quad \times \left[\langle G | \bar{H}^{(x)} \hat{R} | 0 \rangle - E_{\text{EOM}}^\chi \langle G | \hat{R} | 0 \rangle + \langle G | \bar{H} | Q \rangle \langle Q | \hat{R} \hat{T}^\chi | 0 \rangle \right] \\ &= - \langle 0 | \hat{\Omega}^\perp \hat{R} \hat{T}^\chi | 0 \rangle + \langle 0 | \hat{\Pi} \bar{H}^{(x)} \hat{R} | 0 \rangle - E_{\text{EOM-CCSD}}^\chi \langle 0 | \hat{\Pi} \hat{R} | 0 \rangle \\ &\quad + \langle 0 | \hat{\Pi} \bar{H} | Q \rangle \langle Q | \hat{R} \hat{T}^\chi | 0 \rangle \end{aligned} \quad (36)$$

with $\hat{\Pi}$ defined as,

$$\langle 0 | \hat{\Pi} (\bar{H} - E_{\text{EOM-CCSD}}) | G \rangle = - \langle 0 | \hat{\Omega}^\perp | G \rangle \quad (37)$$

Combining **I** and **II** and expanding $E_{\text{EOM-CCSD}}^\chi$ using (18), we arrive at an expression where the direct dependence on \hat{R}^χ and \hat{L}^χ has been replaced by dependence on \hat{T}^χ and \hat{H}^χ (via $\bar{H}^{(x)}$),

$$\begin{aligned} \mathbf{I} + \mathbf{II} &= \left[\langle 0 | (\hat{L} \hat{\Sigma}^\perp - \hat{\Omega}^\perp \hat{R}) \hat{T}^\chi | 0 \rangle + \langle 0 | \hat{L} \bar{H} | Q \rangle \langle Q | \hat{Y} \hat{T}^\chi | 0 \rangle \right. \\ &\quad \left. + \langle 0 | \hat{\Pi} \bar{H} | Q \rangle \langle Q | \hat{R} \hat{T}^\chi | 0 \rangle - \varepsilon \langle 0 | \hat{L} \bar{H} | Q \rangle \langle Q | \hat{R} \hat{T}^\chi | 0 \rangle \right] \end{aligned}$$

$$\begin{aligned}
& + \left[\langle 0 | \hat{L}\bar{H}^{(x)}\hat{Y} | 0 \rangle + \langle 0 | \hat{\Pi}\bar{H}^{(x)}\hat{R} | 0 \rangle - \varepsilon \langle 0 | \hat{L}\bar{H}^{(x)}\hat{R} | 0 \rangle \right] \\
& = \mathbf{III}' + \mathbf{IV}' \tag{38}
\end{aligned}$$

$$\varepsilon = \langle 0 | (\hat{\Pi}\hat{R} + \hat{L}\hat{Y}) | 0 \rangle \tag{39}$$

Note that based on the assumptions above, $\varepsilon = 0$. However, we keep ε in the following derivation for completeness.

The additional terms in \mathbf{III}' can now be added to \mathbf{III} ,

$$\begin{aligned}
\mathbf{III} + \mathbf{III}' & = \langle 0 | \hat{L}_3\hat{V}\hat{R}_1\hat{T}_2^x | 0 \rangle + \langle 0 | (1 - \delta - \varepsilon)\hat{L}\bar{H} | Q \rangle \langle Q | \hat{R}\hat{T}^x | 0 \rangle + \delta \langle 0 | \bar{H}\hat{T}^x | 0 \rangle \\
& + \langle 0 | (\hat{L}\hat{\Sigma}^\perp - \hat{\Omega}^\perp\hat{R})\hat{T}^x | 0 \rangle + \langle 0 | \hat{L}\bar{H} | Q \rangle \langle Q | \hat{Y}\hat{T}^x | 0 \rangle \\
& + \langle 0 | \hat{\Pi}\bar{H} | Q \rangle \langle Q | \hat{R}\hat{T}^x | 0 \rangle \\
& = \langle 0 | \hat{\Xi}\hat{T}^x | 0 \rangle \tag{40}
\end{aligned}$$

$$\begin{aligned}
\langle 0 | \hat{\Xi} | G \rangle & = \langle 0 | \hat{L}_3\hat{V}\hat{R}_1 | D \rangle + \langle 0 | (1 - \delta - \varepsilon)\hat{L}\bar{H} | Q \rangle \langle Q | \hat{R} | G \rangle + \delta \langle 0 | \bar{H} | G \rangle \\
& + \langle 0 | (\hat{L}\hat{\Sigma}^\perp - \hat{\Omega}^\perp\hat{R}) | G \rangle + \langle 0 | \hat{L}\bar{H} | Q \rangle \langle Q | \hat{Y} | G \rangle \\
& + \langle 0 | \hat{\Pi}\bar{H} | Q \rangle \langle Q | \hat{R} | G \rangle \tag{41}
\end{aligned}$$

Differentiation of the \hat{T} amplitude equations (2) yields an expression for $\langle G | \hat{T}^x | 0 \rangle$, where a pseudo-inverse is no longer required due to the fact that while $E_{\text{CCSD}} = \langle 0 | \bar{H} | 0 \rangle$ is an eigenvalue of $\langle P | \bar{H} | P \rangle$, removal of the reference determinant in $\langle G | \bar{H} - E_{\text{CCSD}} | G \rangle$ prevents singularity,

$$\langle G | \hat{T}^x | 0 \rangle = - \langle G | \bar{H} - E_{\text{CCSD}} | G \rangle^{-1} \langle G | \bar{H}^{(x)} | 0 \rangle \tag{42}$$

Using this definition we introduce a final set of de-excitation amplitudes \hat{Z} ,

$$\begin{aligned}
\mathbf{III} + \mathbf{III}' & = - \langle 0 | \hat{\Xi} | G \rangle \langle G | \bar{H} - E_{\text{CCSD}} | G \rangle^{-1} \langle G | \bar{H}^{(x)} | 0 \rangle \\
& = \langle 0 | \hat{Z}\bar{H}^{(x)} | 0 \rangle
\end{aligned}$$

$$= \mathbf{IV}'' \quad (43)$$

$$\langle 0 | \hat{\mathcal{Z}}(\bar{H} - E_{\text{CCSD}}) | G \rangle = - \langle 0 | \hat{\Xi} | G \rangle \quad (44)$$

Finally, the remaining terms \mathbf{IV}' and \mathbf{IV}'' from above can be combined with \mathbf{IV} to yield the total gradient expression,

$$\begin{aligned} E_{\text{EOM-CCSD}^*}^{\chi} &= \mathbf{IV} + \mathbf{IV}' + \mathbf{IV}'' \\ &= \langle 0 | \hat{\Pi} \bar{H}^{(\chi)} \hat{R} | 0 \rangle + \langle 0 | \hat{L} \bar{H}^{(\chi)} \hat{\Upsilon} | 0 \rangle \\ &\quad + (1 - \delta - \varepsilon) \langle 0 | \hat{L} \bar{H}^{(\chi)} \hat{R} | 0 \rangle + \langle 0 | (\delta + \hat{\mathcal{Z}}) \bar{H}^{(\chi)} | 0 \rangle \\ &\quad + \langle 0 | \hat{L} \hat{V}^{\chi} \hat{R}_3 | 0 \rangle + \langle 0 | \hat{L}_3 (\hat{V}^{\chi} \hat{R}_2 + \hat{V}^{\chi} \hat{T}_2 \hat{R}_1) | 0 \rangle \\ &\quad + \langle 0 | \hat{L}_3 \hat{F}^{\chi} \hat{R}_3 | 0 \rangle \end{aligned} \quad (45)$$

$$= \sum_p D_p^p (\epsilon_p)^{\chi} + \sum_{pqrs} \Gamma_{rs}^{pq} (v_{rs}^{pq})^{\chi} \quad (46)$$

where $\epsilon_p = f_p^p$. The one- and two-particle density matrices D_q^p and Γ_{rs}^{pq} can be then be constructed from the various amplitudes and then processed using standard techniques such as in the computation of the CCSD(T) gradient.^{26,49}

3 Results

The analytic gradients of EOMEE-CCSD* have been implemented for closed-shell reference determinants in the development version of the CFOUR program package.⁴⁶ In this section, we discuss the validation of our implementation and demonstrate the illustrative application of analytic EOMEE-CCSD* gradients to a set of excited states. In the geometry optimization, the following convergence thresholds were used, denoted using the relevant CFOUR keywords: SCF_CONV = 10^{-10} , CC_CONV = 10^{-9} , LINEQ_CONV = 10^{-8} , ESTATE_CONV = 10^{-8} , GEO_MAX_STEP = 50 a.u., and GEO_CONV = 10^{-7} , except where indicated.

3.1 Validation

The excited states of formaldehyde have been extensively investigated both experimentally⁵⁰ and theoretically.^{51–56} In addition, its small system size makes it a great candidate for validating the correctness of our implementation against numerical differentiation. The $1^1A_2(n \rightarrow \pi^*)$ valence excited state is investigated here. The ground state geometry is obtained from the QUEST2 dataset,⁵⁷ which has been optimized at the CC3/aug-cc-pVTZ level. The computed EOM-CCSD* gradients (with the aug-cc-pVDZ basis) using both the analytic gradient we implemented and finite differences of energies agree well with each other. The differences between the numerical and analytic values for the individual gradient components were, in all cases, less than 10^{-6} a.u. (see Table 1 in the Supporting Information), which confirmed the correctness of our implementation.

It has been established that the 1^1A_2 state exhibits a non-planar equilibrium geometry.^{50,51,56} Consequently, C_s symmetry is employed during optimization. The optimized geometries and adiabatic excitation energies are summarized in Table 1. The optimized geometries are compared to lower-level EOM-CCSD and higher-level EOM-CCSDT. To facilitate comparison, experimental data are also included.^{58–61} As expected, optimized geometries with EOM-CCSDT are in better agreement with the experimental data. One finds ≤ 0.01 Å difference in the C–O bond and C–H bonds, 0.4° and 2.1° difference in the angle and out-of-plane dihedral, respectively.

TABLE 1. Optimized geometry of $n \rightarrow \pi^*$ excited state of formaldehyde with cc-aug-pVTZ basis set.

	EOM-CCSD	EOM-CCSD*	EOM-CCSDT	Expt.
r_{CO} (Å)	1.306	1.343	1.331	1.323 ^a
r_{CH} (Å)	1.091	1.089	1.093	1.103 ^a
\angle_{COH} ($^\circ$)	119.0	121.0	118.5	118.1 ^a
Out of plane dihedral ($^\circ$)	30.4	27.8	36.1	34.0 ^a
T_e (eV)	3.72	3.12	3.06	3.50 ^b

a) Ref. 59.

b) Ref. 60.

TABLE 2. Harmonic vibrational frequencies (ω), infrared intensities (I) for the $n \rightarrow \pi^*$ excited state of formaldehyde with cc-aug-pVDZ. Numbering of normal modes follows the assignment in the ground state.

Mode	EOM-CCSD		EOM-CCSD*		EOM-CCSDT		Expt. ^a
	ω	I	ω	I	ω	I	ω
$\omega_1(A')$	3143.1	6.4	3054.4	0.5	3011.5	3.0	2846
$\omega_2(A')$	1291.7	30.0	1131.7	68.9	1198.1	21.7	1183
$\omega_3(A')$	1362.0	5.1	1364.7	0.7	1342.8	8.2	1293.1
$\omega_4(A')$	427.0	52.2	548.7	38.1	655.8	40.2	124.5 ^b
$\omega_5(A'')$	3260.1	0.3	3176.7	0.0	3121.3	0.0	2968.3
$\omega_6(A'')$	864.6	5.6	921.6	6.3	924.9	6.1	904

(ω_1) C–H stretching; (ω_2) C–O stretching; (ω_3) CH₂ bending; (ω_4) out-of-plane bending; (ω_5) C–H stretching; (ω_6) CH₂ rocking.

a) From ref. 58,61. Frequencies without a decimal point are deduced from combination bands and uncorrected for anharmonicity.

b) The out-of-plane bending mode has a shallow double-well potential which is not well represented by the harmonic model used here.

EOM-CCSD* considerably improves on EOM-CCSD for the C–O bond length, however for other parameters which exhibit smaller changes between EOM-CCSD and EOM-CCSDT, the EOM-CCSD* results do not consistently move in the correct direction. Trends with respect to experimental data outside of the C–O bond are also not clear. Because the C–O elongation is the most significant change, though, the progression structure for C–O stretching in the vibronic spectrum should be better represented. When examining the computed adiabatic excitation energies, a notable decrease in excitation energy arises when comparing the energy calculated by EOM-CCSD to EOM-CCSD* and EOM-CCSDT. The incorporation of triple excitations in the wave function markedly decreases the adiabatic excitation energies. While the reported experimental T_e value lies between the EOM-CCSD and EOM-CCSD* results, the significantly improved agreement with full EOM-CCSDT indicates a better treatment of electron correlation and geometric relaxation, while additional factors such as basis set completeness would be needed to more closely match experiment.

Harmonic vibrational frequencies and infrared intensities have been obtained by numerical differentiation of analytic energy derivatives and dipole moments at the optimized ge-

ometries and are presented in Table 2. From these results, we can confirm that the optimized geometry corresponds to a minimum. The frequencies computed using EOM-CCSD* align closely with those from EOM-CCSDT, displaying a consistent trend converging towards experimental data.

TABLE 3. Optimized geometry of *s*-tetrazine 1^1B_{3u} ($n \rightarrow \pi^*$) state with the basis set cc-pVTZ. Experimental uncertainties in the last significant digit(s) are given in parentheses.

Parameter	r_{CH} (Å)	r_{CN} (Å)	r_{NN} (Å)	\angle_{HCN} (°)	T_e (eV)
Ground state	1.078	1.336	1.323	116.6	
EOM-CCSD	1.077	1.328	1.312	119.4	2.513
EOM-CCSD*	1.077	1.329	1.319	119.2	1.760
CASSCF ^a	1.067	1.329	1.305	121.4	
CASPT2 ^a	1.073	1.333	1.321	121.5	
Mk-MRCCSD ^b		1.325	1.309		2.642
Expt. ^c	1.063	1.324	1.349	123.2	2.136 ^d
Expt. ^e		1.358(10)	1.28(2)	118.5(14)	

a) Ref. 62

b) Ref. 63

c) Ref. 64

d) In solid benzene, Ref. 65

e) Ref. 66

3.2 $n \rightarrow \pi^*$ states of *s*-tetrazine

Excited states of *s*-tetrazine are of great interest in the scientific community, as neatly summarized in the introduction of the work by Angeli.⁶⁷ The ground state geometry was obtained from the QUEST2 dataset,⁵⁷ which has been optimized at the CC3/aug-cc-pVTZ level. In this study, we focus on the two lowest excited singlet states of B_{3u} and B_{2g} symmetry. The B_{3u} $n \rightarrow \pi^*$ excited state is predominantly characterized by the configuration where a single electron is promoted from the highest occupied molecular orbital b_{3g} to the lowest unoccupied molecular orbital a_u . Previous research has demonstrated that the first excited state exhibits D_{2h} symmetry,⁶² thus guiding our optimization search to only symmetric structures. The optimized geometries and adiabatic excitation energies are succinctly presented

in Table 3. Consistent with previous studies,^{62,63,68} the change in geometry upon electronic excitation is small. While minimal disparities are noted in the optimized geometries between the EOM-CCSD and EOM-CCSD* calculations, there is a small but consistent elongation in the aromatic bond lengths when going from EOM-CCSD to EOM-CCSD*, in opposition to the general contraction of all bonds relative to the ground state. As previously observed, the inclusion of triple excitations substantially reduces the adiabatic excitation energy by 0.75 eV. For comparison, results from additional theoretical studies and experimental findings are included in Table 3.

The B_{2g} $n \rightarrow \pi^*$ excited state is characterized by a mixed configuration of single excitation $4b_{2u} \rightarrow 1a_u$ and double excitation $1b_{1g}3b_{3g} \rightarrow 1a_u1a_u$.⁶⁷ The optimized geometries are summarised in Table 4. In contrast to the B_{3u} excited state where small contractions of all bonds upon excitation are predicted, the B_{2g} excited state relaxes to a geometry with a ≥ 0.13 Å elongation of the N–N bond length and a ≥ 0.015 Å contraction of the C–N bond length. The elongation of the N–N bond can be partially explained by the excitation from bonding $1b_{1g}$ π orbital to the anti-bonding $1a_u$ π orbital. Similar to previous observations, EOM-CCSD* results in larger aromatic bond lengths compared to EOM-CCSD. The triples correction reduces the adiabatic excitation energy by 0.917 eV. This larger drop in energy upon introduction of triples likely reflects the increased double-excitation character in the excited state.

TABLE 4. Optimized geometry of *s*-tetrazine 1^1B_{2g} ($n \rightarrow \pi^*$) state mixed with double excitation with basis set cc-pVTZ.

Parameter	r_{CH} (Å)	r_{CN} (Å)	r_{NN} (Å)	\angle_{HCN} (°)	T_e (eV)
Ground state	1.078	1.336	1.323	116.6	
EOM-CCSD	1.081	1.319	1.453	117.2	5.162
EOM-CCSD*	1.081	1.321	1.456	117.1	4.245

3.3 $1^1A'$ state of cytosine

Cytosine, as one of the building blocks of life, has evoked keen interest in multiple areas.⁶⁹ It has been the motivation of experimental and theoretical efforts to characterize the nature and the properties of the lowest electronically excited states.^{16,69–75} The lowest bright singly-excited state, which is of $\pi \rightarrow \pi^*$ character, is of interest in this work. It is recognized that the optimization of excited states frequently leads to relaxed non-planar geometry.^{69,76} Thus C_1 symmetry is used during optimization. Cytosine presents a major challenge to numerical differentiation in terms of computational cost, as it has 33 internal degrees of freedom (and typically the numerical gradient for all 36 non-translational degrees of is calculated). Here, the ground state geometry is optimized at the MP2/cc-pVTZ level, while the excited state is optimized with the smaller cc-pVDZ basis set. The optimized geometries are summarized in Table 5, and the molecular structure of cytosine is shown in Figure 1. For EOM-CCSD, only geometries with RMS force convergence below 10^{-5} a.u. are presented, and are constrained to a planar geometry. Continuous unconstrained optimization results in significant distortion of the ring structure, making convergence and accurate assignment challenging, particularly due to mixing with the lowest $n \rightarrow \pi^*$ state. For EOM-CCSD*, geometries with RMS force convergence below 10^{-7} a.u. are presented. The more facile convergence of EOM-CCSD* could be due to the more accurate relative energies of the $\pi \rightarrow \pi^*$ and $n \rightarrow \pi^*$ states which sensitively controls the strength of the pseudo-Jahn-Teller (PJT) effect and hence the extent of electronic mixing.⁴² EOM-CCSD and EOM-CCSD* results show consistent trends in bond length changes. While the C_6-N_1 and C_6-N_8 bonds contract, all other bonds exhibit elongation. Aligning with prior research,^{71,74,77} the decay of the $\pi \rightarrow \pi^*$ state involves the carbonyl bond stretching and the pyramidalization of C_{10} and N_8 . Further frequency calculation confirmed it as a minimum (see Table 3 in Supporting information). The largest differences in bond lengths between EOM-CCSD and EOM-CCSD* are on the order of 0.06 Å, while bond angles differ by as much as 9.3° (although the bond angle differences are likely overstated due to the restriction of the EOM-CCSD geometry to planar).

TABLE 5. Optimized bond lengths (r , Å), bond angles (\angle , °), and dihedral angles (ϕ , °) of the cytosine $\pi \rightarrow \pi^*$ state with basis set cc-pVDZ. EOM-CCSD RMS forces are converged to 10^{-5} a.u., see SI for convergence details; EOM-CCSD* RMS forces are converged to 10^{-7} a.u.

Parameter	Ground state	EOM-CCSD	EOM-CCSD*
$r_{\text{C}_2-\text{N}_1}$	1.314	1.417	1.440
$r_{\text{N}_3-\text{C}_2}$	1.354	1.376	1.401
$r_{\text{H}_4-\text{N}_3}$	1.000	1.008	1.020
$r_{\text{H}_5-\text{N}_3}$	1.004	1.009	1.021
$r_{\text{C}_6-\text{N}_1}$	1.373	1.323	1.289
$r_{\text{O}_7-\text{C}_6}$	1.218	1.269	1.331
$r_{\text{N}_8-\text{C}_6}$	1.414	1.410	1.383
$r_{\text{H}_9-\text{N}_8}$	1.008	1.015	1.014
$r_{\text{C}_{10}-\text{N}_8}$	1.351	1.384	1.411
$r_{\text{H}_{11}-\text{C}_{10}}$	1.080	1.089	1.091
$r_{\text{C}_{12}-\text{C}_{10}}$	1.355	1.436	1.420
$r_{\text{H}_{13}-\text{C}_{12}}$	1.077	1.094	1.096
$\angle_{\text{N}_1-\text{C}_2-\text{N}_3}$	117.0	112.2	112.5
$\angle_{\text{C}_2-\text{N}_3-\text{H}_4}$	121.8	122.0	112.7
$\angle_{\text{C}_2-\text{N}_3-\text{H}_5}$	118.0	117.8	110.1
$\angle_{\text{C}_2-\text{N}_1-\text{C}_6}$	120.0	116.1	114.5
$\angle_{\text{N}_1-\text{C}_6-\text{O}_7}$	125.2	123.5	121.9
$\angle_{\text{N}_1-\text{C}_6-\text{N}_8}$	116.1	123.6	125.8
$\angle_{\text{C}_6-\text{N}_8-\text{H}_9}$	115.0	115.5	117.0
$\angle_{\text{C}_6-\text{N}_8-\text{C}_{10}}$	123.8	121.8	118.4
$\angle_{\text{N}_8-\text{C}_{10}-\text{H}_{11}}$	117.0	118.7	118.6
$\angle_{\text{N}_8-\text{C}_{10}-\text{C}_{12}}$	119.8	115.9	115.2
$\angle_{\text{C}_{10}-\text{C}_{12}-\text{H}_{13}}$	121.4	119.1	119.6
$\phi_{\text{N}_1-\text{C}_2-\text{N}_3-\text{H}_4}$	180.0	180.0	155.0
$\phi_{\text{N}_1-\text{C}_2-\text{N}_3-\text{H}_5}$	0.0	0.0	31.7
$\phi_{\text{C}_6-\text{N}_1-\text{C}_2-\text{N}_3}$	180.0	180.0	163.1
$\phi_{\text{C}_2-\text{N}_1-\text{C}_6-\text{O}_7}$	180.0	180.0	177.8
$\phi_{\text{C}_2-\text{N}_1-\text{C}_6-\text{N}_7}$	0.0	0.0	3.1
$\phi_{\text{N}_1-\text{C}_6-\text{N}_8-\text{H}_9}$	180.0	180.0	178.7
$\phi_{\text{N}_1-\text{C}_6-\text{N}_8-\text{C}_{10}}$	0.0	0.0	18.1
$\phi_{\text{C}_6-\text{N}_8-\text{C}_{10}-\text{H}_{11}}$	180.0	180.0	155.3
$\phi_{\text{C}_6-\text{N}_8-\text{C}_{10}-\text{C}_{12}}$	0.0	0.0	-22.6
$\phi_{\text{N}_8-\text{C}_{10}-\text{C}_{12}-\text{H}_{13}}$	180.0	180.0	171.5

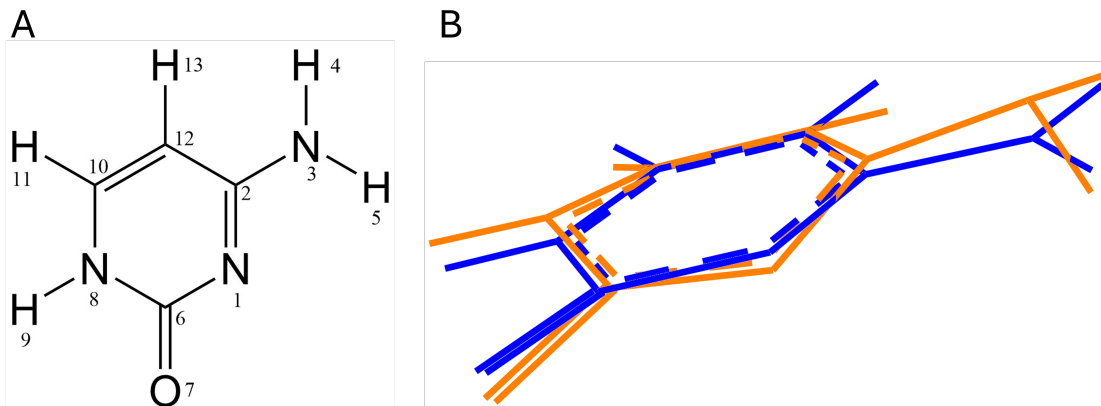


FIGURE 1. Cytosine structures. (A) Cytosine structure labeled with atom indices. (B) The geometric comparison between the ground state (blue) and optimized excited state with EOM-CCSD* (orange), molecules are in the same orientation as shown in A.

4 Conclusion

It has been shown that the effect of triple excitations is important to achieving ~ 0.1 eV accuracy of transition energies.⁷³ Despite numerous variants that approximately integrate triples effects into EOM-CCSD which have emerged over the years, the absence of analytic gradients remains a challenge. In response, this study introduces the formulation and implementation of analytic nuclear gradients for EOMEE-CCSD*.

We showcase the applicability and efficiency of this advancement through demonstrative applications on formaldehyde, *s*-tetrazine, and cytosine systems.

By streamlining the development and implementation of analytic gradient theory for this method, our work not only facilitates in-depth investigations with better accuracy but also substantially broadens the horizons for formulating analytic gradients and consistent properties for complex electronic structure methods spanning both the ground and excited states.

Acknowledgement

This work was supported by the US Department of Energy under grant DOE-SC0022893, and in part by the US National Science Foundation under grant CHE-2143725. All calculations were performed on the ManeFrame III computing system at SMU.

Supporting Information

The following electronic supplementary information files are available from the publisher's website:

- SI.pdf: Supplementary information tables for the formaldehyde and cytosine calculations.
- geometries.xlsx: Relevant geometries from this work in Cartesian coordinates.

References

- (1) Gozem, S.; Luk, H. L.; Schapiro, I.; Olivucci, M. Theory and Simulation of the Ultrafast Double-Bond Isomerization of Biological Chromophores. *Chemical Reviews* **2017**, *117*, 13502–13565.
- (2) Chakraborty, P.; Karsili, T. N. V.; Marchetti, B.; Matsika, S. Mechanistic insights into photoinduced damage of DNA and RNA nucleobases in the gas phase and in bulk solution. *Faraday Discussions* **2018**, *207*, 329–350.
- (3) Kaloni, T. P.; Giesbrecht, P. K.; Schreckenbach, G.; Freund, M. S. Polythiophene: From Fundamental Perspectives to Applications. *Chemistry of Materials* **2017**, *29*, 10248–10283.
- (4) Zhang, J. Z.; Reisner, E. Advancing photosystem II photoelectrochemistry for semi-artificial photosynthesis. *Nature Reviews Chemistry* **2019**, *4*, 6–21.

- (5) Lischka, H.; Nachtigallová, D.; Aquino, A. J. A.; Szalay, P. G.; Plasser, F.; Machado, F. B. C.; Barbatti, M. Multireference Approaches for Excited States of Molecules. *Chemical Reviews* **2018**, *118*, 7293–7361.
- (6) Olsen, J. The CASSCF method: A perspective and commentary. *International Journal of Quantum Chemistry* **2011**, *111*, 3267–3272.
- (7) Andersson, K.; Malmqvist, P. A.; Roos, B. O.; Sadlej, A. J.; Wolinski, K. Second-order perturbation theory with a CASSCF reference function. *The Journal of Physical Chemistry* **1990**, *94*, 5483–5488.
- (8) Angeli, C.; Cimiraglia, R.; Malrieu, J.-P. N-electron valence state perturbation theory: a fast implementation of the strongly contracted variant. *Chemical Physics Letters* **2001**, *350*, 297–305.
- (9) Angeli, C.; Cimiraglia, R.; Evangelisti, S.; Leininger, T.; Malrieu, J.-P. Introduction of n-electron valence states for multireference perturbation theory. *The Journal of Chemical Physics* **2001**, *114*, 10252–10264.
- (10) Angeli, C.; Cimiraglia, R.; Malrieu, J.-P. n-electron valence state perturbation theory: A spinless formulation and an efficient implementation of the strongly contracted and of the partially contracted variants. *The Journal of Chemical Physics* **2002**, *117*, 9138–9153.
- (11) Bartlett, R. To Multireference or not to Multireference: That is the Question? *International Journal of Molecular Sciences* **2002**, *3*, 579–603.
- (12) Watson, M. A.; Chan, G. K.-L. Excited States of Butadiene to Chemical Accuracy: Reconciling Theory and Experiment. *Journal of Chemical Theory and Computation* **2012**, *8*, 4013–4018.

- (13) Stanton, J. F. Many-body methods for excited state potential energy surfaces. I. General theory of energy gradients for the equation-of-motion coupled-cluster method. *The Journal of Chemical Physics* **1993**, *99*, 8840–8847.
- (14) Krylov, A. I. Spin-Flip Equation-of-Motion Coupled-Cluster Electronic Structure Method for a Description of Excited States, Bond Breaking, Diradicals, and Triradicals. *Accounts of Chemical Research* **2005**, *39*, 83–91.
- (15) Musiał, M.; Bartlett, R. J. Addition by subtraction in coupled cluster theory. II. Equation-of-motion coupled cluster method for excited, ionized, and electron-attached states based on the nCC ground state wave function. *Journal of Chemical Physics* **2007**, *127*, 024106.
- (16) Serrano-Andrés, L.; Merchán, M. Quantum chemistry of the excited state: 2005 overview. *Journal of Molecular Structure: THEOCHEM* **2005**, *729*, 99–108.
- (17) Gauss, J.; Stanton, J. F.; Bartlett, R. J. Coupled-cluster open-shell analytic gradients: Implementation of the direct product decomposition approach in energy gradient calculations. *The Journal of Chemical Physics* **1991**, *95*, 2623–2638.
- (18) Gauss, J.; Stanton, J. F. Analytic CCSD(T) second derivatives. *Chemical Physics Letters* **1997**, *276*, 70–77.
- (19) Gauss, J.; Stanton, J. F. Analytic gradients for the coupled-cluster singles, doubles, and triples (CCSDT) model. *The Journal of Chemical Physics* **2002**, *116*, 1773–1782.
- (20) Hratchian, H. P.; Schlegel, H. B. *Theory and Applications of Computational Chemistry*; Elsevier, 2005; pp 195–249.
- (21) Kállay, M.; Gauss, J.; Szalay, P. G. Analytic first derivatives for general coupled-cluster and configuration interaction models. *The Journal of Chemical Physics* **2003**, *119*, 2991–3004.

- (22) Koch, H.; Jensen, H. J. A.; Jørgensen, P.; Helgaker, T.; Scuseria, G. E.; Schaefer, H. F. Coupled cluster energy derivatives. Analytic Hessian for the closed-shell coupled cluster singles and doubles wave function: Theory and applications. *The Journal of Chemical Physics* **1990**, *92*, 4924–4940.
- (23) Lee, T. J.; Rendell, A. P. Analytic gradients for coupled-cluster energies that include noniterative connected triple excitations: Application to cis- and trans-HONO. *The Journal of Chemical Physics* **1991**, *94*, 6229–6236.
- (24) Watts, J. D.; Gauss, J.; Bartlett, R. J. Open-shell analytical energy gradients for triple excitation many-body, coupled-cluster methods: MBPT(4), CCSD+T(CCSD), CCSD(T), and QCISD(T). *Chemical Physics Letters* **1992**, *200*, 1–7.
- (25) Watts, J. D.; Gauss, J.; Bartlett, R. J. Coupled-cluster methods with noniterative triple excitations for restricted open-shell Hartree–Fock and other general single determinant reference functions. Energies and analytical gradients. *The Journal of Chemical Physics* **1993**, *98*, 8718–8733.
- (26) Scuseria, G. E. Analytic evaluation of energy gradients for the singles and doubles coupled cluster method including perturbative triple excitations: Theory and applications to FOOF and Cr2. *The Journal of Chemical Physics* **1991**, *94*, 442–447.
- (27) Yamaguchi, Y.; Schaefer, H. F. Analytic Derivative Methods in Molecular Electronic Structure Theory: A New Dimension to Quantum Chemistry and its Applications to Spectroscopy. 2011; <https://doi.org/10.1002/9780470749593.hrs006>.
- (28) Busch, T.; Esposti, A. D.; Werner, H.-J. Analytical energy gradients for multiconfiguration self-consistent field wave functions with frozen core orbitals. *The Journal of Chemical Physics* **1991**, *94*, 6708–6715.
- (29) Page, M.; Saxe, P.; Adams, G. F.; Lengsfeld, B. H. Multireference CI gradients and MCSCF second derivatives. *The Journal of Chemical Physics* **1984**, *81*, 434–439.

- (30) Shepard, R. Geometrical energy derivative evaluation with $|\text{scpiMRCIi}/\text{scpi}|$ wave functions. *International Journal of Quantum Chemistry* **1987**, *31*, 33–44.
- (31) Vlasisavljevich, B.; Shiozaki, T. Nuclear Energy Gradients for Internally Contracted Complete Active Space Second-Order Perturbation Theory: Multistate Extensions. *Journal of Chemical Theory and Computation* **2016**, *12*, 3781–3787.
- (32) Stanton, J. F.; Gauss, J. Analytic energy derivatives for ionized states described by the equation-of-motion coupled cluster method. *The Journal of Chemical Physics* **1994**, *101*, 8938–8944.
- (33) Stanton, J. F.; Gauss, J. Analytic energy gradients for the equation-of-motion coupled-cluster method: Implementation and application to the HCN/HNC system. *The Journal of Chemical Physics* **1994**, *100*, 4695–4698.
- (34) Stanton, J. F.; Gauss, J. Analytic energy derivatives for the equation-of-motion coupled-cluster method: Algebraic expressions, implementation and application to the S 1 state of HFCO. *Theoretica Chimica Acta* **1995**, *91*, 267–289.
- (35) Levchenko, S. V.; Wang, T.; Krylov, A. I. Analytic gradients for the spin-conserving and spin-flipping equation-of-motion coupled-cluster models with single and double substitutions. *The Journal of Chemical Physics* **2005**, *122*.
- (36) Pieniazek, P. A.; Bradforth, S. E.; Krylov, A. I. Charge localization and Jahn–Teller distortions in the benzene dimer cation. *The Journal of Chemical Physics* **2008**, *129*.
- (37) Wladyslawski, M.; Nooijen, M. *Advances in Quantum Chemistry Volume 49*; Elsevier, 2005; p 1–101.
- (38) Watts, J. D.; Bartlett, R. J. The inclusion of connected triple excitations in the equation-of-motion coupled-cluster method. *The Journal of Chemical Physics* **1994**, *101*, 3073–3078.

- (39) Watts, J. D.; Bartlett, R. J. Economical triple excitation equation-of-motion coupled-cluster methods for excitation energies. *Chemical Physics Letters* **1995**, *233*, 81–87.
- (40) Watts, J. D.; Bartlett, R. J. Iterative and non-iterative triple excitation corrections in coupled-cluster methods for excited electronic states: the EOM-CCSDT-3 and EOM-CCSD(\tilde{T}) methods. *Chemical Physics Letters* **1996**, *258*, 581–588.
- (41) Sattelmeyer, K. W.; Stanton, J. F.; Olsen, J.; Gauss, J. A comparison of excited state properties for iterative approximate triples linear response coupled cluster methods. *Chemical Physics Letters* **2001**, *347*, 499–504.
- (42) Stanton, J. F.; Gauss, J. A simple correction to final state energies of doublet radicals described by equation-of-motion coupled cluster theory in the singles and doubles approximation. *Theoretica Chimica Acta* **1996**, *93*, 303–313.
- (43) Christiansen, O.; Koch, H.; Jørgensen, P. Response functions in the CC3 iterative triple excitation model. *The Journal of Chemical Physics* **1995**, *103*, 7429–7441.
- (44) Koch, H.; Christiansen, O.; Jørgensen, P.; Sanchez de Merás, A. M.; Helgaker, T. The CC3 model: An iterative coupled cluster approach including connected triples. *The Journal of Chemical Physics* **1997**, *106*, 1808–1818.
- (45) Noga, J.; Bartlett, R. J. The full CCSDT model for molecular electronic structure. *The Journal of Chemical Physics* **1987**, *86*, 7041–7050.
- (46) Matthews, D. A.; Cheng, L.; Harding, M. E.; Lipparini, F.; Stopkiewicz, S.; Jagau, T.-C.; Szalay, P. G.; Gauss, J.; Stanton, J. F. Coupled-cluster techniques for computational chemistry: The CFOUR program package. *J. Chem. Phys.* **2020**, *152*, 214108, Publisher: American Institute of Physics.
- (47) Hirata, S. Higher-order equation-of-motion coupled-cluster methods. *The Journal of Chemical Physics* **2004**, *121*, 51–59.

- (48) Saeh, J. C.; Stanton, J. F. Application of an equation-of-motion coupled cluster method including higher-order corrections to potential energy surfaces of radicals. *The Journal of Chemical Physics* **1999**, *111*, 8275–8285.
- (49) Hald, K.; Halkier, A.; Jørgensen, P.; Coriani, S.; Hättig, C.; Helgaker, T. A Lagrangian, integral-density direct formulation and implementation of the analytic CCSD and CCSD(T) gradients. *The Journal of Chemical Physics* **2003**, *118*, 2985–2998.
- (50) Moule, D. C.; Walsh, A. D. Ultraviolet spectra and excited states of formaldehyde. *Chemical Reviews* **1975**, *75*, 67–84.
- (51) Merchán, M.; Roos, B. O. A theoretical determination of the electronic spectrum of formaldehyde. *Theoretica Chimica Acta* **1995**, *92*, 227–239.
- (52) Hachey, M.; Bruna, P.; Grein, F. The Spectroscopy of Formaldehyde. *Journal of Molecular Spectroscopy* **1996**, *176*, 375–384.
- (53) Bruna, P. J.; Hachey, M. R.; Grein, F. Benchmark ab initio calculations of formaldehyde, H₂CO. *Journal of Molecular Structure: THEOCHEM* **1997**, *400*, 177–221.
- (54) Del Bene, J. E.; Gwaltney, S. R.; Bartlett, R. J. Base Properties of H₂CO in the Excited $1n \rightarrow \pi^*$ State. *The Journal of Physical Chemistry A* **1998**, *102*, 5124–5127.
- (55) Dallos, M.; Müller, T.; Lischka, H.; Shepard, R. Geometry optimization of excited valence states of formaldehyde using analytical multireference configuration interaction singles and doubles and multireference averaged quadratic coupled-cluster gradients, and the conical intersection formed by the $^1B_1(\sigma-\pi^*)$ and $^1A_1(\pi-\pi^*)$ states. *The Journal of Chemical Physics* **2001**, *114*, 746–757.
- (56) LISCHKA, H.; DALLOS, M.; SHEPARD, R. Analytic MRCI gradient for excited states: formalism and application to the $n-\pi^*$ valence- and $n-(3s, 3p)$ Rydberg states of formaldehyde. *Molecular Physics* **2002**, *100*, 1647–1658.

- (57) Loos, P.-F.; Boggio-Pasqua, M.; Scemama, A.; Caffarel, M.; Jacquemin, D. Reference Energies for Double Excitations. *Journal of Chemical Theory and Computation* **2019**, *15*, 1939–1956.
- (58) Job, V.; Sethuraman, V.; Innes, K. The 3500 transition of formaldehyde-h₂, d₂, and h_d. *Journal of Molecular Spectroscopy* **1969**, *30*, 365–426.
- (59) Jensen, P.; Bunker, P. The geometry and the inversion potential function of formaldehyde in the and electronic states. *Journal of Molecular Spectroscopy* **1982**, *94*, 114–125.
- (60) Lessard, C. R.; Moule, D. C. The assignment of the Rydberg transitions in the electronic absorption spectrum of formaldehyde. *The Journal of Chemical Physics* **1977**, *66*, 3908–3916.
- (61) Clouthier, D. J.; Ramsay, D. A. The Spectroscopy of Formaldehyde and Thioformaldehyde. *Annual Review of Physical Chemistry* **1983**, *34*, 31–58.
- (62) Schütz, M.; Hutter, J.; Lüthi, H. P. The molecular and electronic structure of s-tetrazine in the ground and first excited state: A theoretical investigation. *The Journal of Chemical Physics* **1995**, *103*, 7048–7057.
- (63) Jagau, T.-C.; Gauss, J. Ground and excited state geometries via Mukherjee’s multireference coupled-cluster method. *Chemical Physics* **2012**, *401*, 73–87.
- (64) Innes, K. Approximate energy of the $1A_u(\pi^*n)$ electronic state of s-tetrazine. *Journal of Molecular Spectroscopy* **1988**, *129*, 140–144.
- (65) Meyling, J.; Van Der Werf, R.; Wiersma, D. Excited state geometry of and radiationless processes in the lowest $B3u(n\pi^*)$ singlet state of s-tetrazine. *Chemical Physics Letters* **1974**, *28*, 364–372.
- (66) Smalley, R. E.; Wharton, L.; Levy, D. H.; Chandler, D. W. The fluorescence excitation

- spectrum of s-tetrazine cooled in a supersonic free jet. *Journal of Molecular Spectroscopy* **1977**, *66*, 375–388.
- (67) Angeli, C.; Cimiraglia, R.; Cestari, M. A multireference n-electron Valence State Perturbation Theory study of the electronic spectrum of s-tetrazine. *Theoretical Chemistry Accounts* **2009**, *123*, 287–298.
- (68) Stanton, J. F.; Gauss, J. The first excited singlet state of s-tetrazine: A theoretical analysis of some outstanding questions. *The Journal of Chemical Physics* **1996**, *104*, 9859–9869.
- (69) Crespo-Hernández, C. E.; Cohen, B.; Hare, P. M.; Kohler, B. Ultrafast Excited-State Dynamics in Nucleic Acids. *Chemical Reviews* **2004**, *104*, 1977–2020.
- (70) Shukla, M.; Mishra, P. A gas phase ab initio excited state geometry optimization study of thymine, cytosine and uracil. *Chemical Physics* **1999**, *240*, 319–329.
- (71) Blancafort, L.; Robb, M. A. Key Role of a Threefold State Crossing in the Ultrafast Decay of Electronically Excited Cytosine. *The Journal of Physical Chemistry A* **2004**, *108*, 10609–10614.
- (72) Tajti, A.; Fogarasi, G.; Szalay, P. G. Reinterpretation of the UV Spectrum of Cytosine: Only Two Electronic Transitions? *ChemPhysChem* **2009**, *10*, 1603–1606.
- (73) Szalay, P. G.; Watson, T.; Perera, A.; Lotrich, V. F.; Bartlett, R. J. Benchmark Studies on the Building Blocks of DNA. 1. Superiority of Coupled Cluster Methods in Describing the Excited States of Nucleobases in the Franck–Condon Region. *The Journal of Physical Chemistry A* **2012**, *116*, 6702–6710.
- (74) Triandafillou, C. G.; Matsika, S. Excited-State Tautomerization of Gas-Phase Cytosine. *The Journal of Physical Chemistry A* **2013**, *117*, 12165–12174.

- (75) Yaghoubi Jouybari, M.; Liu, Y.; Improta, R.; Santoro, F. Ultrafast Dynamics of the Two Lowest Bright Excited States of Cytosine and 1-Methylcytosine: A Quantum Dynamical Study. *Journal of Chemical Theory and Computation* **2020**, *16*, 5792–5808.
- (76) Lobsiger, S.; Trachsel, M. A.; Frey, H.-M.; Leutwyler, S. Excited-State Structure and Dynamics of Keto–Amino Cytosine: The $1\pi\pi^*$ State Is Nonplanar and Its Radiationless Decay Is Not Ultrafast. *The Journal of Physical Chemistry B* **2013**, *117*, 6106–6115.
- (77) Ismail, N.; Blancafort, L.; Olivucci, M.; Kohler, B.; Robb, M. A. Ultrafast Decay of Electronically Excited Singlet Cytosine via a π , π^* to nO , π^* State Switch. *Journal of the American Chemical Society* **2002**, *124*, 6818–6819.

TOC Graphic

